

MIT Open Access Articles

White-light scanning interferometer for absolute nano-scale gap thickness measurement

The MIT Faculty has made this article openly available. **Please share** how this access benefits you. Your story matters.

Citation: Xu, Zhiguang, Vijay Shilpiekandula, Kamal Youcef-toumi, and Soon Fatt Yoon. White-light Scanning Interferometer for Absolute Nano-scale Gap Thickness Measurement. Optics Express 17, no. 17 (August 11, 2009): 15104. © 2009 Optical Society of America

As Published: <http://dx.doi.org/10.1364/OE.17.015104>

Publisher: Optical Society of America

Persistent URL: <http://hdl.handle.net/1721.1/79715>

Version: Final published version: final published article, as it appeared in a journal, conference proceedings, or other formally published context

Terms of Use: Article is made available in accordance with the publisher's policy and may be subject to US copyright law. Please refer to the publisher's site for terms of use.



White-light scanning interferometer for absolute nano-scale gap thickness measurement

Zhiguang Xu^{1,2,3*}, Vijay Shilpiekandula^{1,3}, Kamal Youcef-toumi^{1,3}, Soon Fatt Yoon^{2,3}

¹ Massachusetts Institute of Technology, 77 Massachusetts Avenue, Cambridge, MA 02139, USA

² School of Electrical & Electronic Engineering, Nanyang Technology University, Singapore 639798

³ Singapore-MIT Alliance, N3.2-01-36, 65 Nanyang Drive, Singapore 637460

*zgxu@mit.edu

Abstract: A special configuration of white-light scanning interferometer is described for measuring the absolute air gap thickness between two planar plates brought into close proximity. The measured gap is not located in any interference arm of the interferometer, but acts as an amplitude-and-phase modulator of the light source. Compared with the common white-light interferometer our approach avoids the influence of the chromatic dispersion of the planar plates on the gap thickness quantification. It covers a large measurement range of from approximate contact to tens of microns with a high resolution of 0.1 nm. Detailed analytical models are presented and signal-processing algorithms based on convolution and correlation techniques are developed. Practical measurements are carried out and the experimental results match well with the analysis and simulation. Short-time and long-time repeatabilities are both tested to prove the high performance of our method.

©2009 Optical Society of America

OCIS codes: (120.4640) Optical instruments; (120.3940) Metrology; (120.0120) Instrumentation, measurement and metrology.

References and links

1. S. E. EVLASOV, "Evaluating the quality of optical surfaces by the width of interference fringes", *Meas. Tech.*, **12**, 942-943, (1969).
2. G. W. Meindersma, C. M. Guijt, and A. B. De Haan, "Water Recycling and Desalination by Air Gap Membrane Distillation", *Environ. Prog.*, **24**, 434-44, (2005).
3. J. M. Li, C. Liu, X. D. Dai, H. H. Chen, Y. Liang, H. L. Sun, H. Tian and X. P. Ding, "PMMA microfluidic devices with three-dimensional features for blood cell filtration", *J. Micromech. Microeng.*, **18**, 095021, (2008).
4. A. Dhinojwala and S. Granick, "Micron-gap rheo-optics with parallel plates", *J. Chem. Phys.*, **107**, 8664-8667, 1997
5. C. Ionescu-Zanetti, J. T. Nevill, D. Di Carlo, K. H. Jeong, and L. P. Lee, "Nanogap capacitors: sensitivity to sample permittivity changes," *J. Appl. Phys.*, **99**, 24305, (2006).
6. A. A. Yu, T. A. Savas, G. S. Taylor, A. Guiseppe-Elie, H. I. Smith, and F. Stellacci, "Supramolecular nanostamping: Using DNA as movable type," *Nano Lett.*, **5**, 1061-1064, (2005).
7. V. Shilpiekandula, "Progress through Mechanics: Small-scale Gaps," *Mech.*, **35**, 3-6, (2006).
8. B. Karp and G. Adam, "Small gap width measurement with a finite X-ray source", *NDT&E International*, **27**, 21-25, (1994)
9. J. K. Kim, M. S. Kim, J. H. Bae, J. H. Kwon, H. B. Lee, and S. H. Jeong, "Gap measurement by position-sensitive detectors", *Appl. Opt.*, **39**, 2584-2591, (2000).
10. D. Clifton, A. R. Mount, G. M. Alder, and D. Jardine, "Ultrasonic measurement of the inter-electrode gap in electrochemical machining", *Int. J. Mach. Tools Manuf.*, **42**, 1259-1267, (2002).
11. <http://www.keyence.com/products/vision/laser/lt9000/lt9000.php>
12. E. E. Moon, P. N. Everett, M. W. Meinhold, M. K. Mondol, and H. I. Smith, "Novel mask-wafer gap measurement scheme with nanometer-level detectivity", *J. Vac. Sci. Technol.*, **B**, **17**, 2698-2702, (1999).
13. E. E. Moon, P. N. Everett, K. Rhee, and H. I. Smith, "Simultaneous measurement of gap and superposition in a precision aligner for x-ray nanolithography", *J. Vac. Sci. Technol.*, **B**, **14**, 3969-3973, (1996).
14. D. C. Flanders and T. M. Lyszczarz, "A precision wide-range optical gap measurement technique", *J. Vac. Sci. Technol.*, **B**, **1**, 1196-1199, (1983).
15. R. L. Johnson, J. R. P. Angel, M. Lioyd-Hart, and G. Z. Angeli, "Miniature instrument for the measurement of gap thickness using poly-chromatic interferometry", *Proc. SPIE Int. Soc. Opt. Eng.*, **3762**, 245-253, (1999).

16. A. Courteville, R. Wilhelm and F. Garcia, "A novel, low coherence fibre optic interferometer for position and thickness measurements with unattained accuracy", *Proc. of SPIE*, **6189**, 618918, (2006).
 17. Y. Yasuno, S. Makita, M. Itoh, and T. Yatagai, "Profilometry with line-field Fourier-domain interferometry", *Opt. Express*, **13**, 695-701, (2005).
 18. A. G. Podoleanu, "Unique interpretation of Talbot Bands and Fourier domain white light interferometry", *Opt. Express*, **15**, 9867-9876, (2007).
 19. U. Schnell, R. Dandliker and S. Gray, "Dispersive white-light interferometry for absolute distance measurement with dielectric multilayer systems on the target" *Opt. Lett.*, **21**, 528-530, (1996).
 20. P. Hlubina, D. Ciprian, J. Lunaek, and M. Ilesnak, "Thickness of SiO₂ thin film on silicon wafer measured by dispersive white-light spectral interferometry", *Appl. Phys. B*, **84**, 511-516, (2006)
 21. G. Coppola, P. Ferraro, M. Iodice and S. D. Nicola, "Method for measuring the refractive index and the thickness of transparent plates with a lateral-shear, wavelength-scanning interferometer", *Appl. Opt.*, **42**, 3882-3887, (2003).
 22. P. Maddaloni, G. Coppola, P. D. Natale, S. D. Nicola, P. Ferraro, M. Gioffré, and M. Iodice, "Thickness measurement of thin transparent plates with a broad-band wavelength scanning interferometer", *IEEE Photonics Technol. Lett.*, **16**, 1349-1351, (2004).
 23. P. A. Flournoy, R. W. McClure and G. Wyntjes, "White-Light Interferometric Thickness Gauge", *App. Opt.*, **11**, 1907-1915, (1972).
 24. J. Zhang, Z. H. Lu, and L. J. Wang, "Precision refractive index measurements of air, N₂, O₂, Ar, and CO₂ with a frequency comb", *Appl. Opt.*, 3143-3151, (2008).
 25. A. V. Oppenheim, A. S. Willsky, and I. T. Young, *Signal and systems*, Prentice-Hall, Englewood Cliffs, N. J. USA, 1983.
 26. Physik Instruments Piezo Stage Catalog, "Nanopositioning / Piezoelectrics", (Physik Instruments 2009) http://www.physikinstrumente.com/en/pdf_extra/2009_PI_Nanopositioning_Systems_Piezo_Stage_Catalog.pdf
 27. M. Gutierrez and K. Youcef-Toumi "Programmable Separation for Biologically Active Molecules", *Proceedings of 2006 ASM, Design Engineering Division*, 119, pp 13-20, (2006).
 28. V. Shilpiekandula and K. Youcef-Toumi, "Modeling and Control of a Programmable Filter for Separation of Biologically Active Molecules," *In Proceedings of American Control Conference*, 1, 394-399, (2005).
-

1. Introduction

A small-scale air gap formed between two planar plates plays an important role in a lot of research and industrial fields. In optical manufacturing the surface quality of the optical plate is usually characterized by observing the interference fringes produced by the air gap between the surveyed surface and a standard one [1]. In environmental science air gap membrane distillation is well developed to purify the water from the process industry [2]. The well-controlled narrow gaps are also deployed for filtering the cells or molecules in biotechnology, pharmaceutical and food industries [3].

Many novel applications require the gap thickness to be precisely measured and controlled. In the application of rheo-optics, a gap with the thickness of tens of microns was formed by two parallel plates for deriving the viscous force constant for polymer flow [4]. To determine the dielectric properties of genomic and proteomic structures, a 300nm gap capacitor was created by timed etching of the capacitor spacer in the dielectric spectroscopy [5]. In supramolecular nano-stamping, a novel replication technique for DNA microarrays, the gap between the master and substrate needs to be reduced to a small value on the order of 10nm, i.e. close to the situation of ideal contact, to make the single-stranded DNA features duplicated [6]. The nm- μ m gap is also helpful in researching the phenomena in the near-field physics, such as radiative heat transfer and quantum-dynamic forces [7].

Many techniques have been successfully developed in the literature for absolute gap thickness quantification. The application of optical geometry combined with X-ray technique was demonstrated in [8] and the measurement by position-sensitive detectors (PSD) was introduced in [9]. In electrochemical machining ultrasound technique was employed to characterize the gap between the tool (the cathode) and workpiece (the anode) [10]. Keyence Co. developed a laser confocal sensor for characterizing multiple-layer structures, which is also suited for gap thickness measurement [11]. In silicon wafer manufacturing the gap between the mask and substrate was scaled and controlled by usage of the diffraction phenomena [12, 13]. Laser interferometer, usually limited to the displacement measurement, was extended to survey the absolute gap thickness by Flanders and Lyszczarz. They used an obliquely incident He-Ne laser to illuminate the gap and obtained its thickness by calculating

the spatial frequency of the interference pattern [14]. Johnson group described a white-light phase-shifting interferometry, where the wavelength in the white light source was selected sequentially by a commercial monochromator to illuminate the gap and the gap thickness was calculated according to the phase shift of each wavelength [15]. White-light scanning interferometer was proposed by FOGALE nanotech Inc. to measure the gap thickness (surface spacing) among optical lens, based on the principle that the white-light interference could be only observed when the optical path length in the reference arm matched the positions of the object surfaces in the measuring arm [16].

While the above-mentioned approaches are widely employed, they have various limitations for the micro-scale or nano-scale gap thickness quantification. Methods using optical geometry, ultrasound technique, and PSD are limited by their micron-level resolution and accuracy. The approach with diffraction phenomena can measure the gap as micro as near to contact, but a grating or checkerboard pattern has to be printed on one of the plates forming the gap, which is not convenient for many cases. Flanders and Lyszczarz's method adopting laser interferometry cannot reach the thickness range less than 20 μm ; furthermore, it requires several structural parameters such as incident angle to be measured precisely. The white-light phase-shifting and spectral interferometry can overcome the dispersion of the gap cavity walls; however, their smallest measured thickness, limited by their principles, is usually a quarter of the coherence length of the light source; furthermore, expensive instruments like commercial high-resolution monochromator or spectrometer are usually needed to separate the wavelength from the light source or from the intensity acquired by the detector [17-22].

The white-light scanning interferometer possesses the high resolution and accuracy, and its structure is not as complicated as the white-light phase-shifting or spectral interferometry. However, its applications in gap thickness measurement is limited by the dispersion of the cover plate of the gap, i. e. the air cavity's wall through which the white light transfers, especially when the cover plate is much thicker than the gap. To overcome this disadvantage a compensate plate with identical thickness and refractive index must be inserted into the reference arm of the interferometer; otherwise, the residual dispersion will influence significantly or even destroy the measurement. This specific requirement is hard to meet in many practical applications, for it needs the thickness and refractive index of the cover plate to be precisely measured simultaneously.

The goal of this paper is to develop a special white-light scanning interferometer which can characterize the nano-scale gap thickness, and more importantly, can overcome the chromatic dispersion of the plates including the gap, making the compensate plate not necessary, nor the quantification of the thickness and refractive index of the cover plate. A special configuration of white-light interferometer was introduced to measure the thickness of transparent films, in which the measured film was not located in any interference arm, but acted as a modulator of the light source [23]. Unfortunately, the advantage of this configuration was not totally disclosed in that application for the measurement was still limited by the dispersion of the film material and thus the minimum measured thickness was tens of microns, making it not attract much attention or find any further applications. Here, we extend this configuration into gap thickness measurement, design a new signal processing algorithm for it and find further advantages. With this progress it not only can be used for air gap thickness measurement, but also provides a new approach for the quantification of the covered (or buried) features in various micro devices.

The rest of this paper is organized as follows. In Section 2 we introduce the experimental configuration and theoretical concept of our method, and derive the fundamental relations. In Section 3, the signal processing algorithm is described and simulated, including the usage of convolution/correlation techniques. Practical measurements are presented in Section 4, where the experimental results are compared with the theoretical simulation for proving the validity of our approach and the short-time and long-time repeatabilities are both examined. In Section 5 the precision analysis and future work are discussed. Section 6 concludes the whole paper.

2. Methodology

2.1 Experimental configuration

The experimental apparatus used in this approach is shown schematically in Fig. 1 (a). White light from a quartz halogen lamp, covering the spectrum from 400nm to 1100nm, is collected into a light guide and collimated by an aperture and a lens. The parallel beam is reflected by a beamsplitter and incident on the gap formed between the two optical plates; here multiple-beam interference takes place. The gap-modulated light is then guided into a Michelson interferometer, with a fixed mirror placed in the reference arm and a PZT (Piezoelectric Transducer) driven mirror in the moving arm. The beams reflected from the two arms are recombined and form the interference intensity, which is measured with a photodetector and transferred via a coaxial cable to a computer for data acquisition, processing, and storage.

As compared with common white-light scanning interferometers, the main difference in this configuration is that the measured gap does not act as one interference arm, but a modulator of the light source by the multiple-beam interference. The consequent advantages will be explained in detail in the following section.

For the plates surrounding the air gap are aligned parallel and the transmitted light beam is collimated, there will be an even light intensity distribution I on the photodetector plane, without any interference pattern. When the moving mirror is driven by the PZT so that the length difference between two interference arms Δ is scanned, the continuous variation of the I will be acquired by the photodetector to form an $I-\Delta$ curve, from which the gap thickness will be eventually derived.

2.2 Basic principle

The multiple beam interference occurring at the gap is illustrated in Fig. 1 (b), where the air gap is surrounded by planar plate 1, the cover plate, and plate 2. Let E_{input} be the complex amplitude of the input beam, and $E_1, E_2, E_3,$ and E_4 the sequentially reflected beams from four different surfaces. A series of r and t denote the reflection and transmission amplitude coefficients at the corresponding surfaces, and their values can be easily calculated by Fresnel equations. h, h_1 and h_2 are the thickness of the gap and the two plates, and n_a, n_1 and n_2 their refractive indexes. According to the practical applications of micro gaps h is much smaller than h_1 and h_2 . The incident angle is represented by α , and the refractive angles in two plates by β and γ .

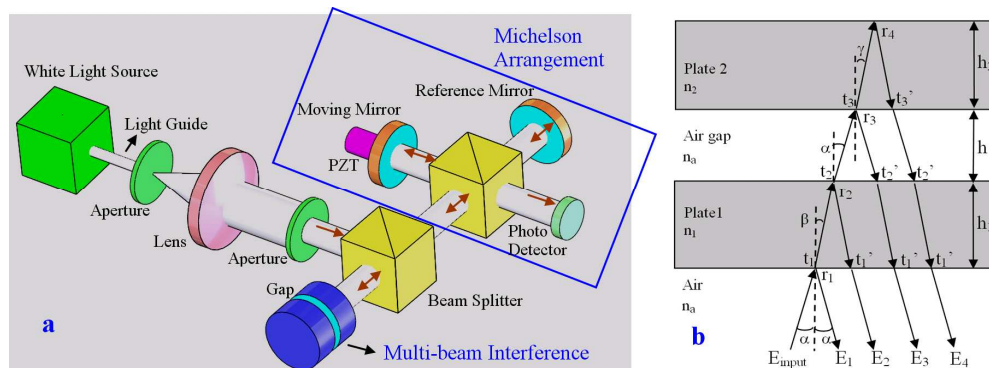


Fig. 1. (a) Schematic of experimental setup to characterize the tiny gap between two planar plates; (b) Modulation of the light source by the multi-beam interference occurring at the gap.

The complex amplitude of each reflected beam is:

$$\begin{aligned}
E_1 &= E_{input} r_1; \\
E_2 &= E_{input} t_1 r_2 t_1' e^{i\varphi_1}; \\
E_3 &= E_{input} t_1 t_2 r_3 t_2' t_1' e^{i(\delta+\varphi_1)}; \\
E_4 &= E_{input} t_1 t_2 t_3 r_4 t_3' t_2' t_1' e^{i(\delta+\varphi_1+\varphi_2)}
\end{aligned} \tag{1}$$

where the phase change δ , φ_1 and φ_2 are:

$$\delta = \frac{2\pi}{\lambda} 2n_a h \cos \alpha; \varphi_1 = \frac{2\pi}{\lambda} 2n_1 h_1 \cos \beta; \varphi_2 = \frac{2\pi}{\lambda} 2n_2 h_2 \cos \gamma; \tag{2}$$

Neglecting the reflections in higher orders due to their little intensity, the sum of the complex amplitude of the reflected beams is written as:

$$\begin{aligned}
E_{gap} &= E_1 + E_2 + E_3 + E_4 \\
&= E_{input} (r_1 + t_1 r_2 t_1' e^{i\varphi_1} + t_1 t_2 r_3 t_2' t_1' e^{i(\delta+\varphi_1)} + t_1 t_2 t_3 r_4 t_3' t_2' t_1' e^{i(\delta+\varphi_1+\varphi_2)})
\end{aligned} \tag{3}$$

Apparently, both the amplitude and phase of the input light are modulated by the gap. In case of vertical incidence, $\alpha = \beta = \gamma = 0$.

According to the characterization of Michelson interferometer, the half transmission of each beamsplitter and the wavelength range covered by the white light source, the final intensity received by the photodetector can be described by formula (4). In this formula a, b, c, d and A are positive constants, and C_1 to C_7 are functions of Δ . The negative sign in C_2, C_3, C_4 , and C_7 is due to the 180 phase shift introduced by reflection at the interface from a low refractive index media to a high one.

$$I = \frac{1}{4} \int_{\lambda_1}^{\lambda_2} I_{gap} \cos\left(1 + \frac{4\pi\Delta}{\lambda}\right) d\lambda = A + C_1 + C_2 + C_3 + C_4 + C_5 + C_6 + C_7$$

with

$$\begin{aligned}
C_1 &= \frac{1}{4} \int_{\lambda_1}^{\lambda_2} (a^2 + b^2 + c^2 + d^2) \cos \frac{4\pi\Delta}{\lambda} d\lambda \\
C_2 &= -\frac{1}{4} \int_{\lambda_1}^{\lambda_2} bc \cos \frac{4\pi(n_a h + \Delta)}{\lambda} d\lambda - \frac{1}{4} \int_{\lambda_1}^{\lambda_2} bc \cos \frac{4\pi(n_a h - \Delta)}{\lambda} d\lambda \\
C_3 &= -\frac{1}{4} \int_{\lambda_1}^{\lambda_2} ab \cos \frac{4\pi[n_1(\lambda)h_1 + \Delta]}{\lambda} d\lambda - \frac{1}{4} \int_{\lambda_1}^{\lambda_2} ab \cos \frac{4\pi[n_1(\lambda)h_1 - \Delta]}{\lambda} d\lambda \\
C_4 &= -\frac{1}{4} \int_{\lambda_1}^{\lambda_2} cd \cos \frac{4\pi[n_2(\lambda)h_2 + \Delta]}{\lambda} d\lambda - \frac{1}{4} \int_{\lambda_1}^{\lambda_2} cd \cos \frac{4\pi[n_2(\lambda)h_2 - \Delta]}{\lambda} d\lambda \\
C_5 &= \frac{1}{4} \int_{\lambda_1}^{\lambda_2} ac \cos \frac{4\pi[n_1(\lambda)h_1 + n_a h + \Delta]}{\lambda} d\lambda + \frac{1}{4} \int_{\lambda_1}^{\lambda_2} ac \cos \frac{4\pi[n_1(\lambda)h_1 + n_a h - \Delta]}{\lambda} d\lambda \\
C_6 &= \frac{1}{4} \int_{\lambda_1}^{\lambda_2} bd \cos \frac{4\pi[n_2(\lambda)h_2 + n_a h + \Delta]}{\lambda} d\lambda + \frac{1}{4} \int_{\lambda_1}^{\lambda_2} bd \cos \frac{4\pi[n_2(\lambda)h_2 + n_a h - \Delta]}{\lambda} d\lambda \\
C_7 &= -\frac{1}{4} \int_{\lambda_1}^{\lambda_2} ad \cos \frac{4\pi[n_1(\lambda)h_1 + n_a h + n_2(\lambda)h_2 + \Delta]}{\lambda} d\lambda \\
&\quad - \frac{1}{4} \int_{\lambda_1}^{\lambda_2} ad \cos \frac{4\pi[n_1(\lambda)h_1 + n_a h + n_2(\lambda)h_2 - \Delta]}{\lambda} d\lambda
\end{aligned} \tag{4}$$

The elements of C_1 to C_7 denote different components in the $I-\Delta$ signal, which is acquired by the photodetector when the PZT drives the moving mirror continuously. A simulated $I-\Delta$ signal by Matlab is presented in Fig. 2, where each C produces one or two local curves and each curve includes a sharp peak with its side lobes, as shown in Fig. 2 (a) and (b). For instance, for C_1 only as Δ equals zero all the $\cos(4\pi\Delta/\lambda)$ functions obtain the maximum 1 for every wavelength, so a peak will occur at the position of $\Delta = 0$, i.e. the position where the PZT translates to make the length of two interference arms equal. The same goes for

$\cos[4\pi(\Delta+n_a h)/\lambda]$ and $\cos[4\pi(\Delta-n_a h)/\lambda]$ in C_2 , so that two symmetrical downward peaks can be observed at $\Delta = n_a h$ and $\Delta = -n_a h$, respectively. As a result, the spacing between the peaks in the local curves denoted by C_1 and C_2 is exactly the value of $n_a h$, and therefore the gap thickness can be determined by measuring this spacing, which forms the basic principle of our method. In normal situation the air refractive index n_a can be considered a consistent of 1.00028 [24], whose variation can be negligible in our experimental environments.

2.3 The influence from dispersion of the plates

(a) For common white-light scanning interferometers

In the common white-light scanning interferometer the measured gap is located in the measuring arm of the interferometer, and a PZT driven moving mirror in the reference arm. Now the intensity acquired by the photodetector will be:

$$I = M_1 + \int_{\lambda_1}^{\lambda_2} M_2 \cos \frac{4\pi\Delta}{\lambda} d\lambda - \int_{\lambda_1}^{\lambda_2} M_3 \cos \frac{4\pi[n_1(\lambda)h_1 - \Delta]}{\lambda} d\lambda \quad (5)$$

$$+ \int_{\lambda_1}^{\lambda_2} M_4 \cos \frac{4\pi[n_1(\lambda)h_1 + n_a h - \Delta]}{\lambda} d\lambda + \dots$$

where M_1 to M_4 are constant values; the third and fourth items in formula (5) result in two local curves in the $I-\Delta$ signal, and the spacing between their peaks is expected to be a measure for the gap thickness. One practical case is simulated in Fig. 3, where a 20 μm air gap is included by a 200- μm -thick cover plate and another 300 μm plate and the cover plate is made of BK7 glass. The two local curves before and after consideration of the dispersion of the cover plate are presented in Fig. 3 (a) and (b) for comparison. In (a) n_1 is given by a constant, the refractive index of BK7 glass for the central wavelength of the light source. In (b) n_1 is a function of λ due to the actual dispersion as in Fig. 3 (d), and now no certain Δ can make the cosine functions in formula (5) get simultaneously the maximum for all the wavelengths. As a result, the widths of the local curves are extended, amplitudes of the peaks are reduced and their positions deviate from the ideal ones. If the cover plate is thicker or the dispersion of the material is more significant, the negative influence of the dispersion will be more evident to make the gap thickness measurement impossible.

(b) For our proposed method

For our presented approach the variation of n_1 and n_2 with λ will not cause any change to the values of C_1 and C_2 in Eq. 4, nor the peak spacing denoting the gap thickness which is completely governed by $n_a h$. Even with significant dispersion in the cover plate, the Central Curve and Side Curve are the same as in Fig. 2 (a) and (b). Therefore, the dispersion of the air cavity's walls does not affect our measurement at all.

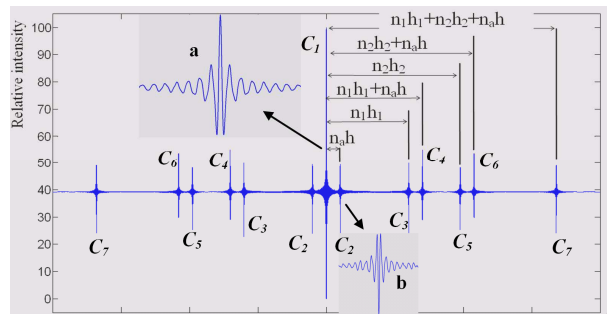


Fig. 2. Simulated $I-\Delta$ signal in which local curves produced by C_1 to C_7 in Eq. 4 are observed with their spacings remarked; a and b show the shapes of the local curves by C_1 and C_2 .

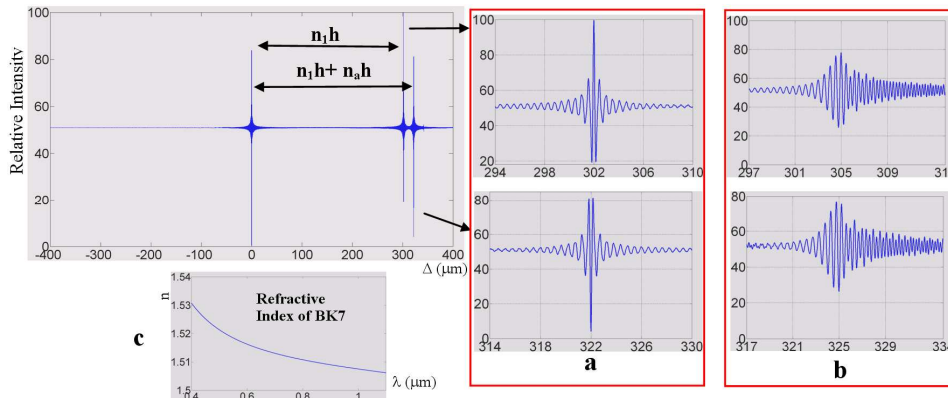


Fig. 3. Simulated $I-\Delta$ signal for the common white-light scanning interferometer. (a) two local curves before consideration of the dispersion of the cover plate; (b) two local curves after considering the dispersion.

3. Signal processing methodology

In micro gap thickness measurement, Δ will be scanned by the PZT in a limited range of tens of microns near $\Delta = 0$; therefore, only the three local curves represented by C_1 and C_2 can be included in the practically obtained $I-\Delta$ signal. Other local curves, too far away from the location of $\Delta = 0$, will not be considered in the following analysis. Now the three local curves generated by C_1 and C_2 are named by Central Curve and Side Curves, and the three peaks dominating the gap thickness measurement are Central Peak and Side Peaks, respectively.

3.1 Signal processing for gap thickness larger than 10 μm

Gap thickness larger than 10 μm can be quantified directly by the spacing between the Central Peak and Side Peak. In practical measurements these peaks are evident enough to be identified by the maximum or minimum value in the acquired $I-\Delta$ signal. (A spare algorithm by calculating the centroid of the local curve to obtain the peak position is also developed.)

Random noise, inevitable in practical experiments, may result in errors in determining the positions of the peaks. Assuming the light intensity incident on the gap I_{input} to be 1W, the random noise with a substantial amplitude of 4mW is simulated and added into the signal, as shown in Fig. 4 (a). The Central and Side Curves are zoomed in (b) and (c), where the noise makes the peak positions hard to identify precisely.

Convolution calculation [25] is applied to address this problem. The simulated Central Peak is specially extracted as in Fig. 4 (d), and the convolution between this peak and the whole signal is calculated. This process, acting as a signal filtering, reduces dramatically the influence of the noise and makes the peak positions much easier to determine. The calculation result is shown in Fig. 4 (e), which almost forms the same curve as the ideal signal without any noise. From the peaks enlarged in (f) and (g), the gap thickness can be precisely achieved as 10 μm .

3.2 Signal processing for gap thickness between 1 μm and 10 μm

The signal simulated for a 2 μm gap is shown in Fig. 5 (a). Now the Central Curve and the Side Curves are close enough to combine partly with one another, and thus the side lobes are added to the peaks to make them deviate from original shapes and shift from ideal locations, especially for the two Side Peaks. In this case calculating the gap thickness only through peak spacing becomes difficult.

To overcome the combination of the Central and Side Curves, an algorithm is designed to subtract the Central Curve from the signal, to make only the side ones left. The concept is as follows. When the gap is very thick so that the spacing between the three local curves is quite

large, the Side Curves will move out of the scanning range of the PZT. As a result, only the Central Curve exists in the scanned $I-\Delta$ signal and thus it can be recorded separately, as shown in Fig. 5 (b). In practical measurements this procedure only needs to be operated for one time before measuring the gaps, thereafter this data can be used as a reference and subtracted from the obtained signals for gaps thinner than $10\ \mu\text{m}$. The signal in Fig. 5 (a) is processed and the data after subtracting the Central Curve is shown in Fig. 6, in which the two Side Peaks return to their ideal locations, $2\ \mu\text{m}$ and $-2\ \mu\text{m}$. Now the gap thickness can be characterized accurately by calculating the half spacing between these two downward peaks. If heavy noise exists in the signal, the convolution calculation introduced in the former section can still be employed.

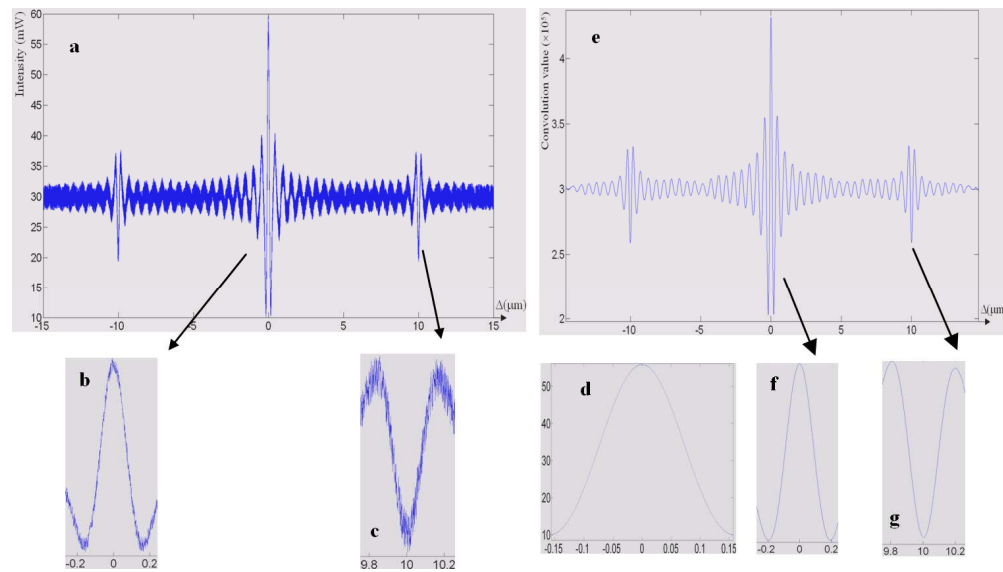


Fig. 4. (a) Random noise with the amplitude of the 4mW is simulated and added into the simulated signal for a $10\ \mu\text{m}$ gap. (b) Central Curve with noise. (c) Side Curve with noise. (e) Simulated Central Peak. (f) Convolution calculation between the simulated Central Peak as in (e) and the whole signal reduces largely the influence of the noise. (f) Central Curve after noise filtering. (g) Side Curve after noise filtering. From (f) and (g) the gap thickness can be easily identified.

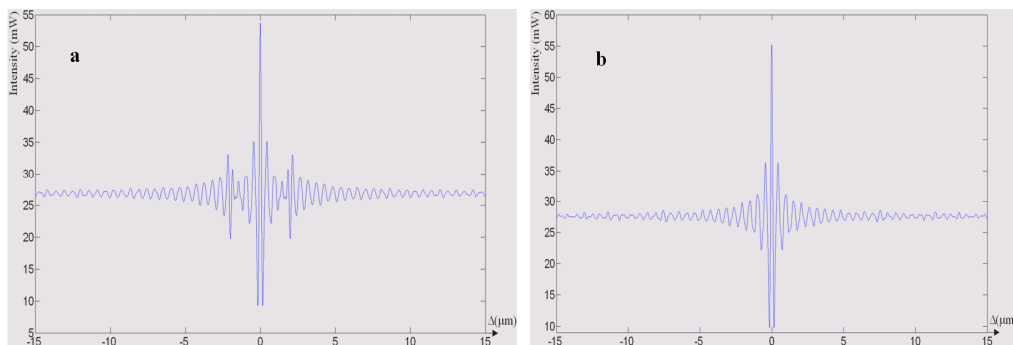


Fig. 5. (a) Simulated signal for a $2\ \mu\text{m}$ gap, in which the three local curves are combined partly to make the gap thickness quantification very difficult; (b) Recorded data for the Central Curve when the gap is thick enough to make the two side peaks go beyond the PZR scanning range.

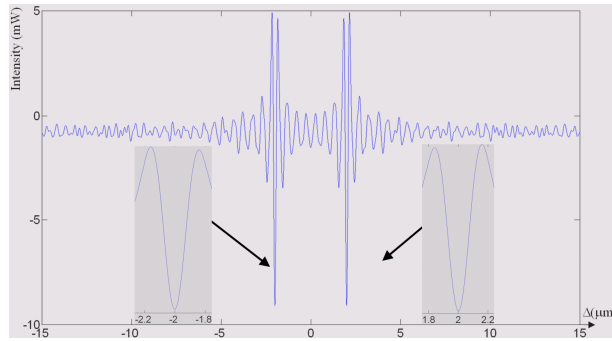


Fig. 6. Simulated signal for a 2 μm gap, in which the Central Curve has been subtracted and the Side Peaks return to their ideal positions.

3.3 Signal processing for gap thickness less than 1 μm

For the gap thickness less than 1 μm the Central Curve is first of all subtracted from the $I-\Delta$ signal. But even after that the Side Peaks still deviate from their ideal locations because now even the two Side Curves are close enough to combine with one another. The simulated curve of a 400 nm gap after subtracting the Central Curve is illustrated in Fig. 7.

Signal matching technique, i.e. the correlation calculation between the acquired signal and the simulated ones in a database, is applied to process this case. The detailed process is as follows. In numerical simulations, we include two Side Curves and vary their distance, i.e. the spacing between two Side Peaks, from 1 nm to 1 μm to obtain their corresponding signals, forming a database for gap thickness from 1 nm to 1 μm . The practically obtained signal, after subtracting the Central Curve, will be compared with the signals in this database by correlation calculation, and the one matching the practical signal best shows the gap thickness.

To establish the database the Side Curve data must be obtained first. From Eq. 4 we know that the Central Curve and Side ones, produced by C_1 and C_2 , have completely the same shape; the only difference exists in their amplitude and orientation (upward or downward). Therefore, if the acquired Central Curve in Fig. 5 (b) is placed upside down, it can be taken as the Side Curve by a ratio; and the influence of this ratio will be removed in the correlation calculation because correlation only cares about the shape of curves.

The $I-\Delta$ signal for a 400 nm gap with a 2mW peak-to-peak random noise is simulated in Fig. 8 (a), and the results of the correlation calculation between it and the curves in the database are illustrated in (b). The gap thickness is determined as 400 nm exactly, from which one can see that the correlation calculation helps finding the gap thickness from the database in a high accuracy, even for cases with heavy noise.

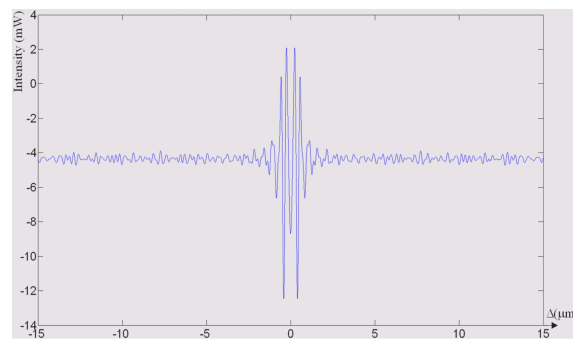


Fig. 7. Simulated signal for a 400 nm gap, in which the central peak has been subtracted and side peaks are so close as to be combined together.

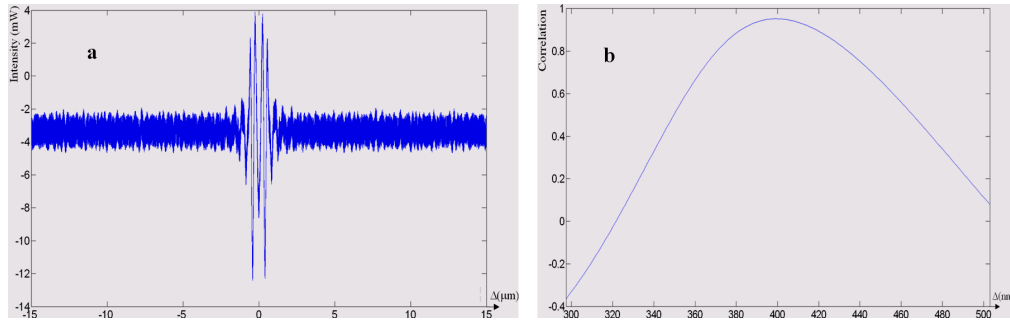


Fig. 8. (a) Simulated curve for a 400 nm gap with 2mW peak-to-peak random noise. (b) Results of the correlation calculation between (a) and the curves in the database.

4. Experiments

4.1 Experimental setup

The experimental setup is shown in Fig. 9 (a), in which 1 is the light guide collecting the white light from the light source (Dolan-Jenner DC-950H); an aperture with selectable diameter is placed in front of the guide to form a point light source; 2 denotes a achromatic lens collimating the light, which also reduces dramatically the chromatic and spherical aberration; 3 is the second aperture dominating the illuminated area of the plates; 4 and 5 are cube beamsplitters with the reflecting surface orientated at 45° angle with the incident beam; 6 the fixed mirror; 7 and 8 are two planar glass plates with nominal flatness $1/20$ wavelength; by using screw-adjusted kinematic mounts the gap included by the two plates can be adjusted to different thickness values for measurement. 9 is the high-speed, high-sensitivity and low-noise photodetector (SD112-42-11-231) from Advanced Photonix, Inc.

To implement the optical alignment of the system a He-Ne laser is employed as a reference. The laser spots reflected from the two surfaces of the gap, or from the reference and moving mirrors, are received at a screen far away, and the complete superposition of the spots indicates the parallelism of the air gap walls and the perpendicularity between the two interference mirrors. To guarantee the performance all the measurement system is set up on a vibration isolated optical table, and the environmental light is shielded to the fullest extent.

Fig. 9 (b) shows the moving mirror driven by a PZT, which is held in a flexure based mechanism manufactured by abrasive water jet machining technique. 1 represents the PZT from PI Company; 2 is the capacitance sensor (ADE Tech Probe 2805) to measure on-line the displacement of PZT, providing a feedback signal to form the close loop control to assure the high accuracy and repeatability of the PZT moving. 3 is the collar holding the mirror, which is connected to 4, the flexure.

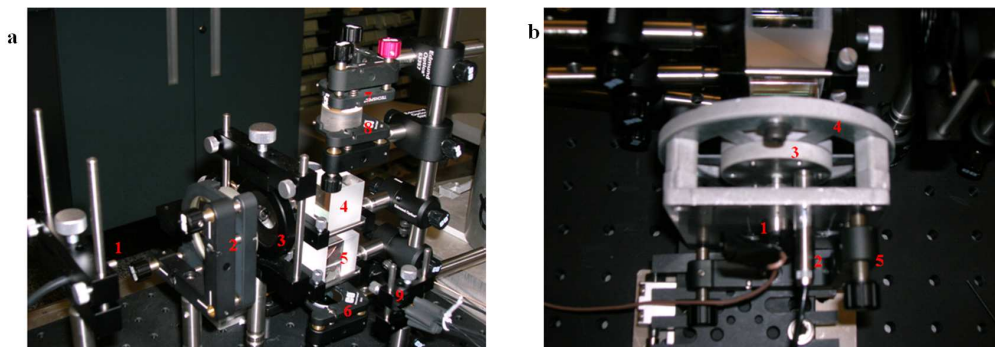


Fig. 9. (a) Experimental setup to measure the gap thickness; (b) Flexure based mechanism to hold the PZT driving the moving mirror.

4. 2 Experimental Data for gaps with different thickness

The method we propose for white light scanning interferometry requires the moving mirror to be scanned in a range of microns and at a sub-nanometer resolution. To this end, we use a piezoelectric scanner in tandem with a flexural mechanism and sensor for closed-loop feedback around the motion scanning stage. Flexural mechanisms driven by piezoelectric actuators are well-known for achieving sub-nanometer resolutions. Piezoelectric actuators with 0.1 nm resolution and 1 nm repeatability are commercially available [26]. While these benefits are in open-loop operation, many closed-loop control algorithms have been developed for improving robust stability and performance. The control aspects of achieving sub-nanometer resolution are beyond the scope of this paper. For these details, the reader is referred to results reported by us in [27, 28]. Closed-loop control for tracking 0.2nm steps of a PZT-driven flexural scanner stage with a capacitance probe is achieved in [28], and therein the details of the control algorithm used are provided. With low-pass filtering of capacitance probe output data, the resolution is demonstrated to be limited to 0.1nm by the filtered RMS-noise of the probe electronics.

In this work, we proceed with the same flexure-based PZT scanning stage used at a closed-loop position resolution of 0.1 nm, and this dictates the measurement resolution of our approach. The measurement range depends on the scanning length of the applied PZT, currently 16 μm ; if larger range is needed an amplification mechanism can be selected, or an electromechanical actuator such as the voice coil motor can be selected.

The experimental signal acquired for a practical gap is shown in Fig. 10 (a-1), in which abscissa axis shows the PZT translation and axis of ordinates the intensity received by the photodetector. Based on our signal processing technique including the convolution calculation, the gap thickness is estimated as 10.1258 μm . For this case the PZT scanning range 16 μm cannot cover all the three local curves, so only the Central Curve and one Side Curve are included in the acquired curve.

In the practically obtained curve the difference between the intensity of the peak and of its side lobes appears not so significant, because the light source does not emit all the wavelengths from 400 nm to 1100 nm by an even ratio, and the same goes for the transmission of the lens and beam splitters, as well as the detection of the photodetector. Taking into account the practical parameters of these components, the theoretical curve for a 10.1258 μm gap is simulated by Matlab and illustrated in Fig. 10 (a-2), from which we can see the high similarity between the practical and simulated results. The correlation between these two signals is calculated as 0.957, verifying the validity of our approach.

By adjusting the fine screws in the kinematic mount and aligning the parallelism of the two plates, two thinner gaps are formed for quantification. Their acquired signals are shown in Fig. 10 (b-1) and (c-1), from which one can see evidently the gap turn thinner gradually. Now the Central Curve and Side ones are close enough to combine partly with each other, especially for the case in Fig. 10 (c-1), so the subtraction of the Central Curve introduced in Section 3.2 is applied, and the gap thicknesses are determined to be 6.3733 μm and 1.6514 μm . The theoretical signals for the two gap thicknesses are also simulated in Fig. 10 (b-2) and (c-2), and the correlation ratios between the experiments and simulations are 0.921 and 0.936, respectively.

Fig. 10 (d-1) shows the acquired signal for gap thickness less than 1 μm , for which both the subtraction of the Central Curve and signal matching technique are applied. The results of the correlation calculation between the acquired signal and the simulated ones in the database are illustrated in (d-2), from which the gap thickness is determined as 494.3 nm.

4. 3 Repeatability of our experiments

To test the short-time repeatability of our approach an air gap with the estimated thickness about 500 nm is measured eight times within one minute. The results from the eight measurements are listed in the first column of Tab. 1 and the SD (Standard Deviation) of the measurements is calculated as 5.8 nm. The long-time repeatability is examined by quantifying

the same gap in one hour with the time spacing of 5 minutes, as shown in the second column in Tab. 1, and the SD is determined as 7.3nm.

Another gap thickness about 5.88 μm is characterized in the same manner. The measurement results are also shown in Tab. 1, with the short-term and long-term SDs calculated to be 7.4 nm and 19.7 nm, respectively. The high repeatability of our approach makes it competent for the practical applications.

5. Discussion

The measurement errors mainly come from four sources. The first one is the influence from the environmental noise. Fortunately, in our approach the gap thickness is determined not directly by the intensity but by the position of the peaks, and convolution/correlation algorithm is developed to process the signal, so the influence of the noise has been dramatically reduced. The second source is the asymmetry of the acquired local curves. The Central Curve and the Side one are not perfectly symmetric about their own middle lines, especially the Central Curve; and on the left of the Central Peak there are more side lobes than on the right. This asymmetry, showing that the light transmitting in the system is not a perfect parallel beam, may induce error in identifying the peak positions. There are several possible sources causing this asymmetry. (1) The collimating lens does not remove all the chromatic and spherical aberrations from the incident beam, making it include convergent or divergent rays. (2) The fixed mirror or the moving one is bent when it is fixed in the mount, making it deviate from a planar surface. The accuracy error of the PZT translation, e.g. error in the repeatability and linearity, and the thermal expansion of the components are other two elements which can also introduce error into the eventual measurement result.

In theory we can characterize gap thickness as small as close to the resolution of our method; however, limited by the practical experimental conditions, e.g. the dust particle concentration in the laboratory and the actual flatness and cleanness of the two plates forming the gap, we did not reach this scale.

The laser interferometry may be a better approach if the gap thickness Δ is limited within half wavelength of the applied laser, for it can achieve sub-nanometer accuracy measurement. For example, for a He-Ne laser interferometer, $\lambda/2$ is 316.4 nm. When the Δ goes beyond this limit there will occur 2π phase ambiguity, i.e. the laser interferometer, when measuring the absolute gap thickness, can not identify Δ from $\Delta + n\lambda/2$, ($n=1, 2, 3\dots$). The measurement range required in many applications is often much larger than hundreds of nanometers, but often tens or hundreds of microns. For these cases the laser interferometer is not suitable. Our approach can cover the gap thickness quantification from approximate contact to tens of microns; if larger range is needed, we just need to use an electromechanical actuator such as the voice coil motor to replace the PZT, with nothing else changed in the setup.

The current verification of our measurement accuracy and the repeatability is based on the high performance of the PZT translation and our data processing; the better approach is to use some reference metrology method, e.g. laser interferometer, or standard sample. Now we are combining our approach into a novel hot-embossing technique, to measure and control the gap between the tool and the sample. In this coming work the accuracy of our approach will be verified by using a laser interferometer, Model SP120 from SIOS Mebtechnik GmbH. This progress will be presented in the future.

In future work we will improve the performance of our interferometer by ameliorating the working environment and updating hardware in our experiments. Currently the gap thickness is adjusted by the three screws in the kinematic mount. A new flexure based mechanism is in development to move the two plates and align their orientation, to realize high-speed, high-resolution and on-line control for the gap thickness.

As part of future work we will apply this approach into the practical hot-embossing machine for manufacturing microfluidic devices, where the gap thickness at three different positions will be characterized on the gap surface simultaneously, for the real-time control of the parallelism of the tool and sample.

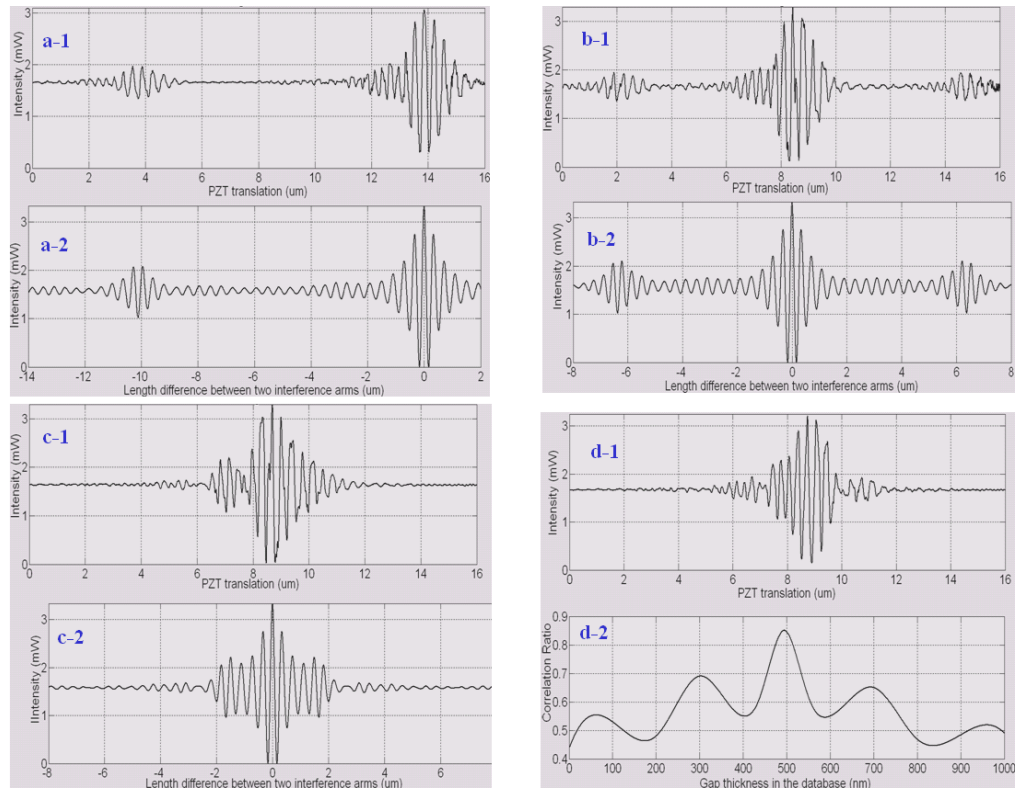


Fig. 10. (a-1), (b-1) and (c-1) are the experimental curves detected by the photodetector for four gaps, from which the gap thickness is determined to be 10.1258 μm , 6.3733 μm , 1.6514 μm and 494.3 nm. (a-2), (b-2) and (c-2) present the simulated signal for the 10.1258 μm , 6.3733 μm , 1.6514 μm gaps with consideration of all the practical parameters; (d-2): Result of the correlation calculation between the experimental data in (d-1) and the simulated signals in the database for gap thicknesses from 1 nm to 1 μm .

TABLE I
MEASUREMENTS FOR EXAMINING THE SHORT-TERM AND LONG-TERM REPEATABILITIES

Gap I		Gap II	
Measurements for short term repeatability (nm)	Measurements for long term repeatability (nm)	Measurements for short term repeatability (μm)	Measurements for long term repeatability (μm)
500.3	490.5	5.8759	5.8858
509.2	509.6	5.8689	5.8910
497.5	497.7	5.8693	5.9087
508.4	507.5	5.8743	5.9021
494.0	500.6	5.8849	5.9029
499.2	503.2	5.8903	5.8782
497.5	495.5	5.8792	5.8621
494.3	506.4	5.8751	5.8725
	493.6		5.8767
	491.0		5.8663
	492.6		5.8546
	511.2		5.8561
	494.8		5.8492

6. Conclusion

We successfully measured nano-scale gap thickness by a special configuration of white-light scanning interferometer, in which the measured gap acts as a modulator of the light source. It overcomes the shortage in the common white-light interferometer, avoids influence of the chromatic dispersion in the plates surrounding the gap, and provides a new approach for the characterizing the covered features such as steps in a variety of micro devices. In this implementation we do not employ any expensive instrument like commercial spectrometer or monochromator, whose prices range from several thousands to tens of thousands \$, but only use common optical components to make the whole cost less than 3K \$. A new signal processing method is developed, with which our approach has the promise to characterize gap thickness from approximate contact to tens of μm . Currently, the measurement resolution is 0.1 nm and the range depends on the scanning range of the applied PZT. Practical experiments are carried out and the results match well with the simulated signals; high short-time and long-time repeatabilities are both proved, which all demonstrate the validity and advantage of our approach.

Acknowledgments

The authors would like to thank the Singapore-MIT Alliance Program for supporting this research. We are indebted to Dr Li Shiguang in Nanyang Technological University, who gave us much help in this work.